Supplementary Information

Deposited and detected molecules, calculated transition states

Table ST1: Names, molecular formulas, skeleton structures, and ball-and-stick structures of molecular species deposited and those formed and detected. Red is an oxygen atom, black is carbon, and white is hydrogen.

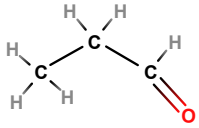
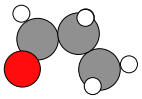
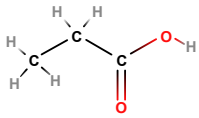
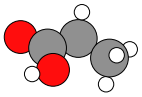
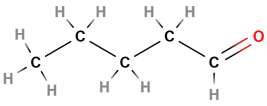
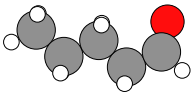
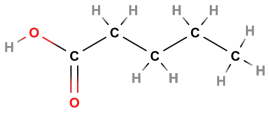
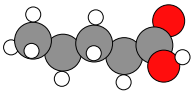
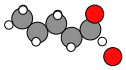
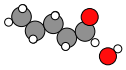
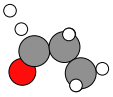
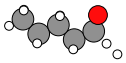
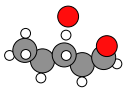
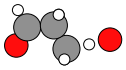
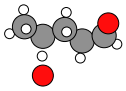
Molecule name	Molecular formula	Skeleton figure	Ball and stick figure
Propanal	CH_3CH_2CHO		
Propanoic acid	CH_3CH_2COOH		
Pentanal	$CH_3(CH_2)_3CHO$		
Pentanoic acid	$CH_3(CH_2)_3COOH$		

Table ST2: Transition states and their ball-and-stick figures for the corresponding geometries of propanal and pentanal. Red is an oxygen atom, black is carbon, and white is hydrogen.

Transition states	Propanal ball-and-stick figure	Pentanal ball-and-stick figure
TS_1		
$TS_{1,OH}$		
$TS_{1,H}$		
$TS_{2,1}$		
$TS_{2,2}$		
$TS_{3,1}$		
$TS_{3,2}$		
$TS_{3,3}$		
$TS_{4,1}$		
$TS_{4,2}$		
$TS_{5,1}$		
$TS_{5,2}$		
$TS_{5,3}$		

Molecule infrared band assignments

Table ST3 shows the infrared (IR) band positions measured for propanal in this work, those found in the literature [1], and the vibrational mode the band is assigned to.

Table ST3: The IR band assignments for propanal, based on previous work [1]

Band position (cm^{-1})	Literature band position (cm^{-1})	Band assignment
2992-2704	2976	CH_3 asymmetric stretch
1742-1687	1732	C=O stretch
1458	1460	CH_3 asymmetric deformation
1392	1392	CH_3 symmetric deformation
1342	1342	CH_2 wagging
1094	1094	CH_3 rocking
857	854	CCC symmetric stretch

Table ST4 shows the IR band positions measured for propanoic acid in this work, those found in the literature [2], and the vibrational mode the band is assigned to.

Table ST4: The IR band assignments for propanoic acid, based on previous work [2]

Band position (cm^{-1})	Literature band position (cm^{-1})	Band assignment
3280-2798	3000	OH stretch
2984	2990	CH_3 asymmetric stretch
1720	1720	C=O stretch
1467	1472	CH_3 asymmetric in-plane bend
1430	1434	OH in-plane bend
1417	1420	CH_2 in-plane bend
1385	1380	CH_3 symmetric in-plane bend
1350	1350	CH_2 wagging
1297	1302	CH_2 twist
1250	1250	C−O stretch
1083	1080	C−C asymmetric stretch
953	930	OH out of plane

Desorption of propanal

In the main text, Figure 2 shows that the temperature-programmed desorption (TPD) measurements of propanal have two desorption peaks. The first is assigned to propanal desorbing from the surface, whereas the second is from desorption elsewhere, likely from the sample holder. To support this assignment, IR scans were conducted during the TPD measurement. The temperature at which this scan is assigned is the temperature of the surface at the midpoint of the scan. The signals of the scans were integrated, and the total integrated signal is plotted against temperature and shown in Supplementary Figure SF1(a).

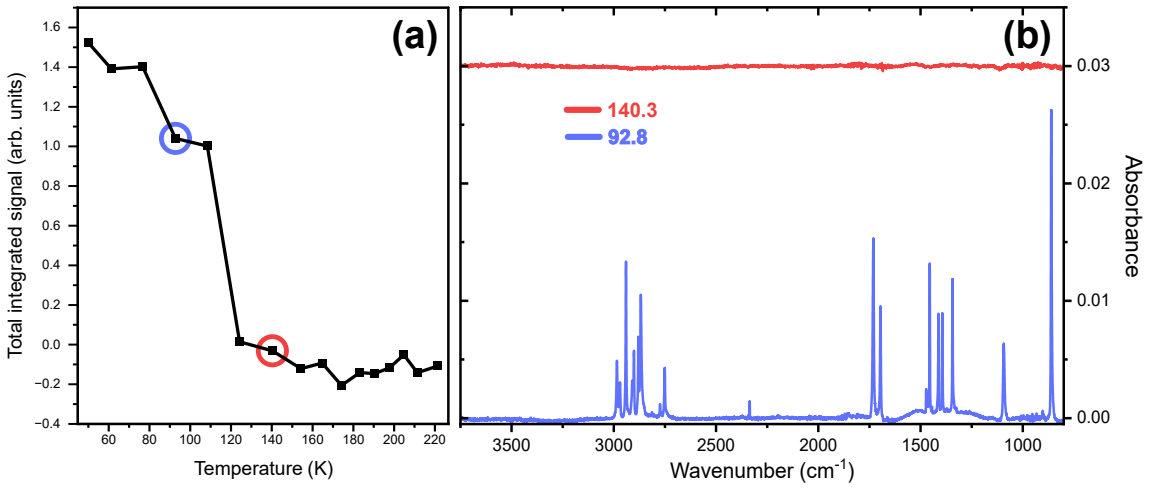


Figure SF1: Shown in (a) is the total integrated signal of the IR spectra taken during a TPD measurement of propanal. The temperature points are the midpoint temperatures of the measurements. Highlighted in blue is the measurement shown in (b) of propanal at 92.8 K, present on the surface. In red is the measurement taken at 140.3 K, showing that at this temperature the propanal has desorbed completely from the gold surface.

The figure shows that the signal decreases sharply at the measurement at 124.2 K. After this point, there is no signal left, and due to the background measurement of the gold being measured at 50 K, at these higher temperatures the signal becomes slightly negative. The decrease in signal at 124.2 K is likely due to the desorption of propanal, meaning it is no longer measured on the surface. This is in agreement with the TPD measurements shown in the main paper.

To ensure that the IR spectra themselves support this, two spectra, one at 92.8 K and another at 140.3 K, are plotted in Supplementary Figure SF1(b). The spectrum at 92.8 K can be seen to have the bands associated with propanal, though at this temperature they have become sharp, indicating that the propanal has become crystalline. The spectrum at 140.3 K shows no trace of the propanal, indicating it has desorbed from the surface

Reactions of Propanoic Acid with O(^3P)

Figure 3 in the main article depicts the energy levels of calculated transition states for reactions between propanal and an O(^3P) atom. This first investigation highlights the primary reaction channels present between the dosed molecule and radicals. Once this primary reaction channel, as in Equation 1, concludes, the potential for further reactions with the propanoic acid should also be considered for further reaction. An almost identical investigation to that performed in the main article was then performed on propanoic acid. An important difference between the reactions considered for the two molecules is that abstraction from the acid group is now also considered: $TS_{1,abstract=O}$ (abstraction of the oxygen from the double CO bond in the acid group) and $TS_{1,abstractH/OH}$ (abstraction of the hydrogen from the hydroxyl in the acid group). Figure SF2 depicts the results of this investigation. Reactions with the acid group are classified by high barriers, particularly with regard to attacking the highly electronegative C=O. Whilst the rest of the considered reactions are less prohibited, there are still no reactions with lower activation energies than 0.25 eV, which when compared to the low activation energy aldehyde reaction channel suggests that further reactions, if present, will be strongly mediated by tunnelling rather than by overcoming the kinetic barrier. As an aside, the transition state energies for hydrogens bonded to the same carbon have in all cases become more split in energy between stereoisomeric sites. This points to the impact of the acid group on the electronic structure of the aldehyde.

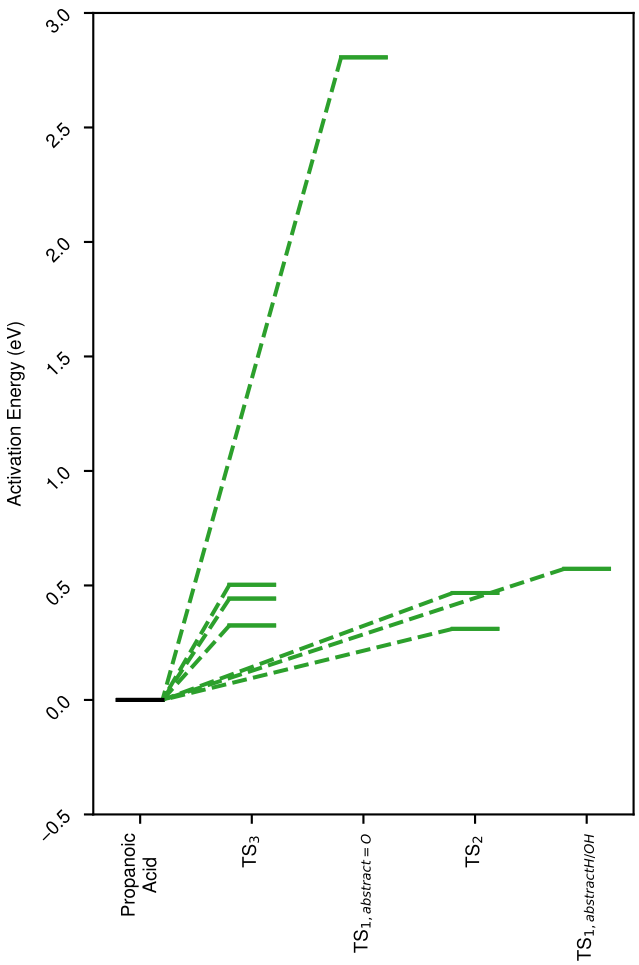


Figure SF2: Depicted in green are the transition state energies of potential hydrogen abstraction reactions of oxygen atoms with propanoic acid. TS_2, and TS_3 (depicted in Figure ST2) indicate hydrogen abstraction reactions from the secondary and tertiary carbons, respectively. $\mathrm{TS}_{1,abstract=O}$ and $\mathrm{TS}_{1,abstractH/OH}$ denote the abstraction of the double bond oxygen from the acid group and abstraction of the hydrogen from the hydroxyl group, respectively. Those with multiple lines corresponding to the same carbon indicate stereoisomerically unique sites.

Reactions of Pentanoic Acid with O(^3P)

In a similar vein to that considered for propanoic acid, further reactions of pentanoic acid with O(^3P) were also considered, with the same methodology. The results of this investigation are shown in Figure SF3, in which the transition state labels follow the naming convention outlined in Table ST2, where the key difference is that the formyl group is replaced with an acid group. As with propanoic acid, the attack by O(^3P) onto the double bond CO of the acid group is highly biased against, as has been omitted from Figure SF3 to improve clarity. The splitting in energy levels between stereoisomeric sites is again larger than for pentanal, with the most substantial effect observed on the carbons closest to the functional group, and the least on those furthest away. TS_2, for example, demonstrates a large between the activation energies for the two sites, corresponding to orientation with the neighbouring hydroxyl group or away from it. The key conclusion from this investigation is, however, that the presence of the acid group on this molecule does not meaningfully alter the abstraction chemistry of O(^3P) such that it might allow substantial further reaction, when contrasted to pentanal.

Methane ($\mathrm{CH_4}$) benchmark

The proposed CCSD(T)-F12/BHANDHLYP was also applied to the hydrocarbon molecule methane, in order to benchmark the performance of this combined hybrid geometry optimisation with coupled cluster

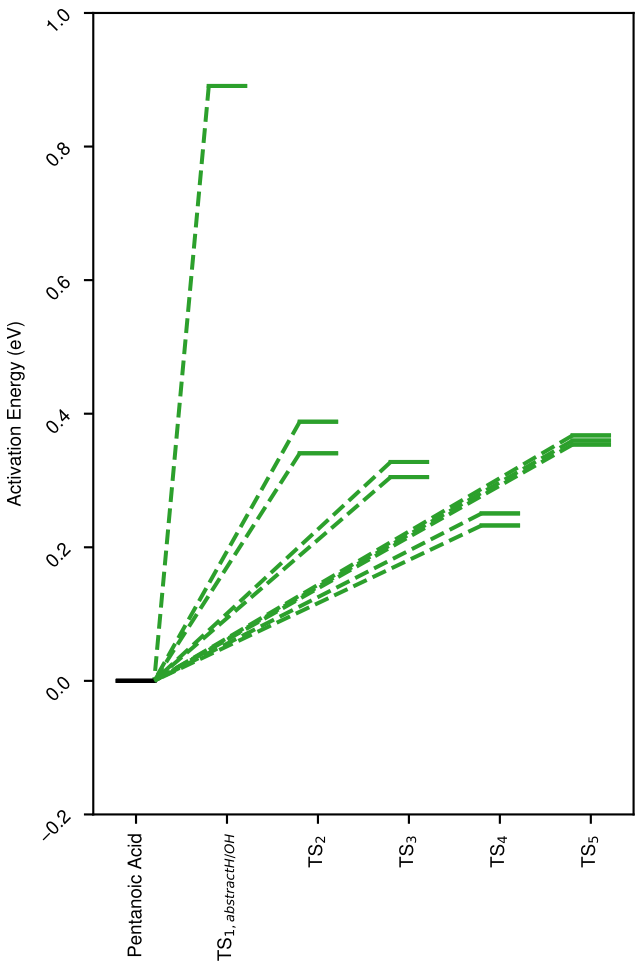


Figure SF3: Depicted in green are the transition state energies of potential hydrogen abstraction reactions of oxygen atoms with pentanoic acid. Those with multiple lines corresponding to the same carbon indicate stereoisomerically unique sites.

refinement approach. A previous multi-reference method study [3] studied the abstraction of hydrogen from methane by O(^3P), and identified an abstraction barrier of 0.54 eV. A different study targeting the same molecule [4], with a single-reference coupled-cluster approach, with geometries derived from a model trained to coupled cluster, obtained a hydrogen abstraction barrier by hydroxyl of 0.22 eV. The resultant barriers when applying CCSD(T)-F12/BHANDHLYP for O(^3P) and OH are 0.50 and 0.21, as seen in SF4. These values are consistent with those previously calculated.

Reactions of propanal with O(^1D)

Throughout the investigation in the main article, only the interactions between triplet spin state (O(^3P)) atoms and hydrocarbons are considered. Previous literature studies linking to conditions in the ISM [5, 6, 7, 8] have investigated reactions with the excited and highly reactive O(^1D) radical as a direct result of the photochemical disassociation of O_2. Each of these studies finds a swathe of barrierless insertion reactions occurring across a range of molecules.

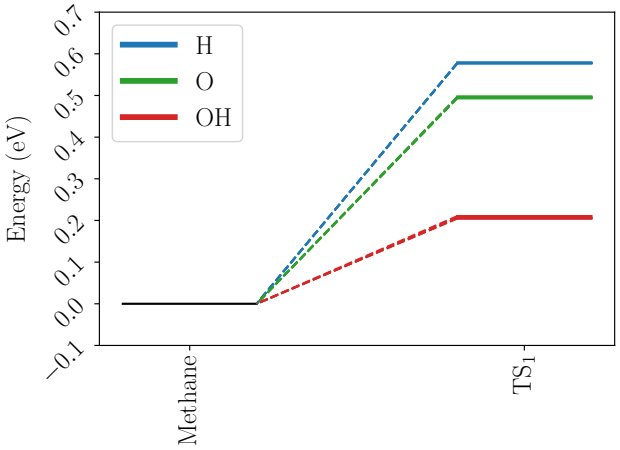


Figure SF4: Reaction activation barriers for abstraction of hydrogen from methane by a hydrogen radical (blue), O(^3P) (green), and by a hydroxyl radical. Only a single abstraction is required per reactant owing to the symmetry of the methane molecule.

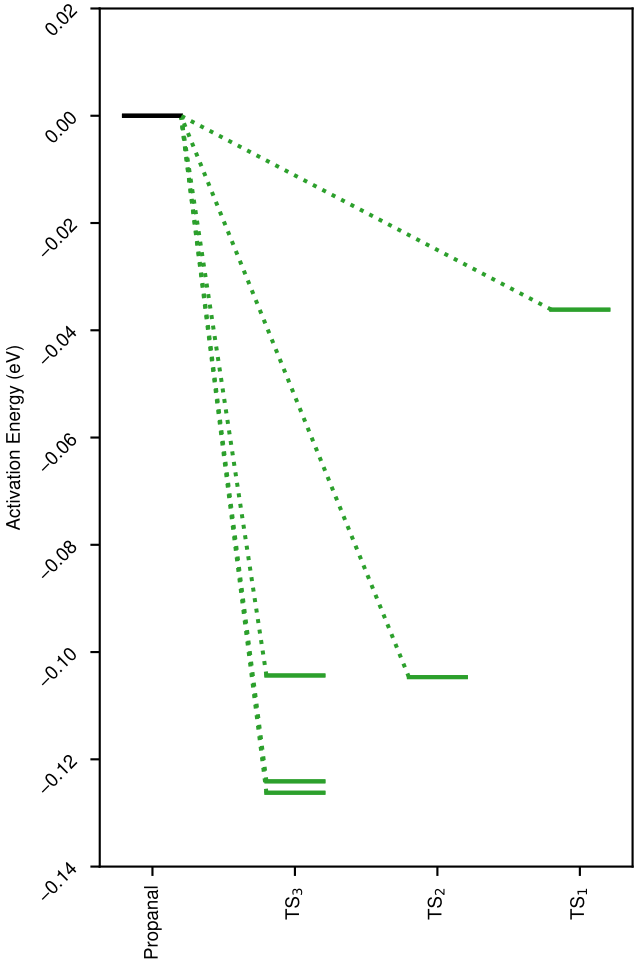


Figure SF5: Reaction energy barriers for O(^1D) with propanal. TS_1, TS_2, and TS_3, indicate reactions with hydrogens bonded with the primary, secondary, and tertiary carbons in propanal, respectively.

Figure SF5 depicts reactions occurring on the singlet energy surface, where geometries and transition

states have been obtained from scratch. Rather than remaining as a radical radical complex after relaxation, as in the case of the triplet energy surface, on the singlet surface the oxygen inserts directly into the C-H bond. Furthermore, in stark contrast to those in Figure 3, each of the activation energies calculated here is less than 0, resulting in a set of effectively barrierless reactions. This is in agreement with the trends observed in previous literature [5, 6, 7, 8]. Therefore, if $O(^1D)$ was present and the driving force for such reactions, it is unlikely that carboxylic acids would be produced as reaction endpoints.

Layer of pentanal exposed to oxygen atoms

Experiments exposing aldehydes to oxygen atoms in the main paper are all conducted as a co-deposition of the aldehyde and oxygen atoms. The experiments were performed this way to increase the IR and QMS signal of the acid products and to prevent layers of H_2O and CO_2 from adsorbing onto the surface and covering the aldehyde such that it could not be processed by the oxygen atoms. However, to ensure that the reaction is occurring on the surface and that the co-deposition has no effect on the chemistry, pentanal was deposited onto the gold substrate and then exposed to oxygen atoms. This experiment is shown in Supplementary Fig SF6.

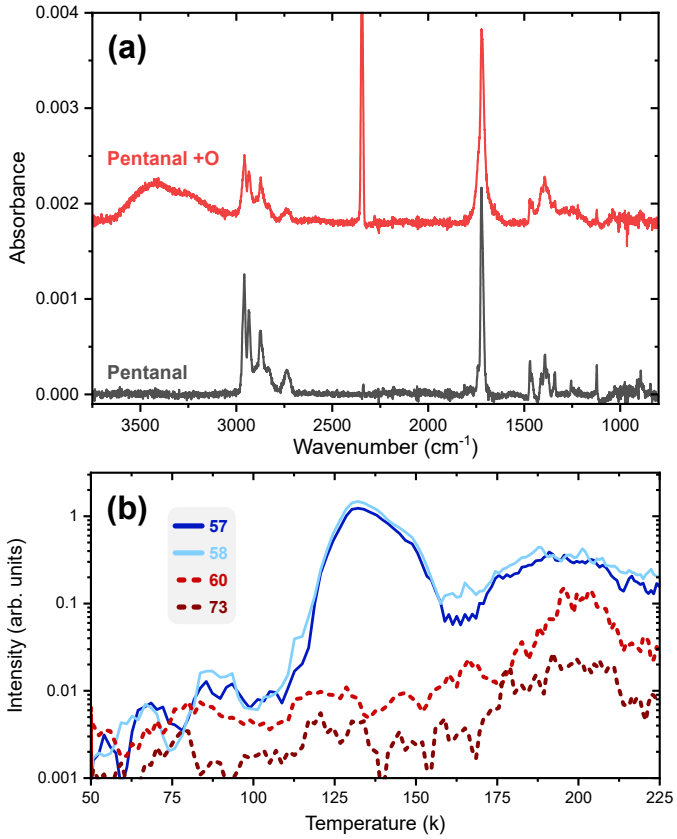


Figure SF6: The IR spectra of pentanal deposited and then after oxygen atom exposure and its corresponding TPD measurement. (a) shows the pentanal deposited onto the gold substrate (grey) and then the spectrum after it has been exposed to oxygen atoms (red). (b) shows the TPD measurement after oxygen atom exposure with characteristic pentanal masses (57 and 58 amu) desorbing at 132 K and pentanoic acid masses 60 and 73 amu desorbing at 198 K.

Supplementary Fig SF6(a) shows the IR spectra of the pentanal (grey) deposition onto the gold substrate before being exposed to oxygen atoms and then after being exposed (red). The as-deposited spectrum is as shown in the main text, but after exposure to oxygen atoms can be seen to have changed. The C=O stretching mode at 1723 cm^{-1} has broadened, similarly to what was observed for the co-dose experiments, and there is a new absorption at 1225 cm^{-1} which corresponds to the C–O stretching mode. These IR bands are expected for pentanoic acid being formed on the surface. There is a broad absorption at 3414 cm^{-1} attributed to the OH stretching mode, which can be due to a combination of pentanoic acid being present and the background deposition of water from the atomic sources.

Supplementary Fig SF6(b) shows the TPD measurement conducted after the layer of pentanal was exposed to oxygen atoms. The characteristic mass fragments of pentanal, 57 and 58 amu [9], can be seen to desorb from the surface at 132 K, as was observed for the co-deposition experiments. At the higher temperature of 198 K, the characteristic mass fragments of pentanoic acid, 60 and 73 amu [10], desorb from the surface, showing that in both co-deposition and layer experiments, the acid is formed through surface, condensed-phase reactions.

Reactions on a highly oriented pyrolytic graphite substrate

All experiments shown in the main article were performed with a gold substrate. This was not expected to contribute to the chemistry and had no catalytic effects. This was especially true with the co-deposition experiments, where the gold was quickly covered, and any potential effects it could have had would be diminished. To show that the gold substrate had no effect on the resulting chemistry, pentanal and its reaction with oxygen atoms when dosed onto a highly oriented pyrolytic graphite (HOPG) substrate were investigated. HOPG was used, as this is expected to be inert. The results of this are presented in Supplementary Fig SF7.

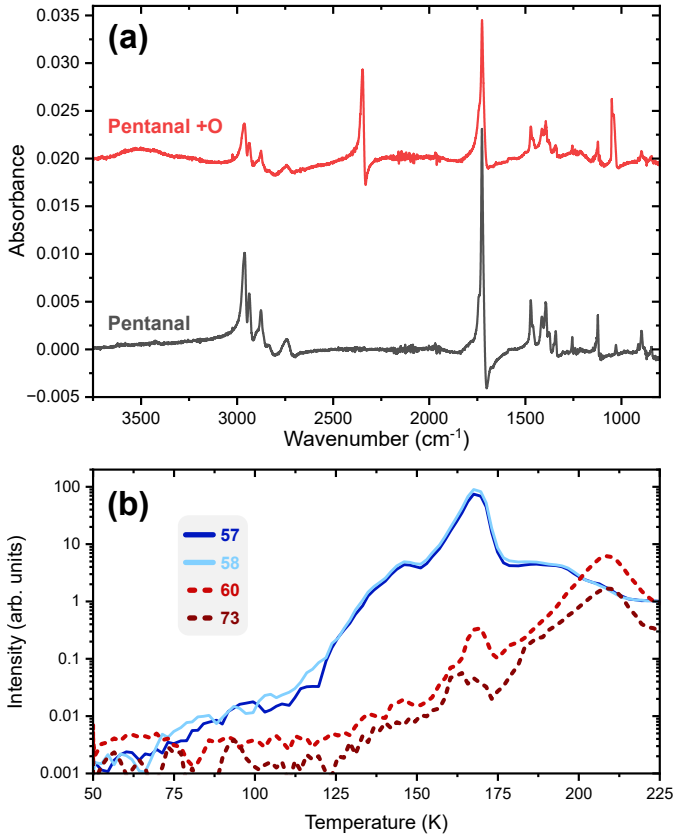


Figure SF7: (a) The IR spectra of pentanal (grey) and pentanal exposed to oxygen atoms (red) with an HOPG substrate. (b) shows the TPD measurement of pentanal exposed to oxygen atoms, with the acid being detected desorbing at 208 K.

Supplementary Fig SF7(a) shows the IR spectra of pentanal deposited onto the HOPG substrate (grey) and its co-dose with oxygen atoms (red). The pentanal deposition spectrum shows all of the expected bands of pentanal, similar to those of pentanal deposited onto gold. Of note are the features that show negative absorption. This is a known effect of using graphite as a substrate [11]. The spectrum of the pentanal exposed to oxygen atoms shows characteristics of an acid being present. There is a broad absorption at 3460 cm^{-1} from OH stretching modes; the C=O stretching mode at 1725 cm^{-1} has broadened, removing the negative feature, and there is a small broad absorption at 1224 cm^{-1} from the C−O stretch.

Supplementary Fig SF7(b) shows the TPD measurements of pentanal exposed to oxygen atoms. The traces show that pentanal desorbs from the surface at 168 K, but that pentanoic acid was formed, as

its mass fragments were recorded desorbing at 208 K. This shows that the substrate did not affect the fundamental chemical reaction taking place to form acids from aldehydes. This, therefore, means it is likely to occur on dust grain surfaces and ices within the ISM.

Oxygen and hydrogen atom co-dose

To measure the effects of both the Hydrogen atom beam source (HABS) and the Oxygen atom beam source (OABS), the gold substrate was exposed to both atomic beams for the same length of time as for the propanal and pentanal experiments. This would allow for the water formation to be observed and see what was outgassed from the hot filaments in the dosers. The results of this measurement, its IR spectrum and TPD measurement, are shown in Supplementary Fig SF8.

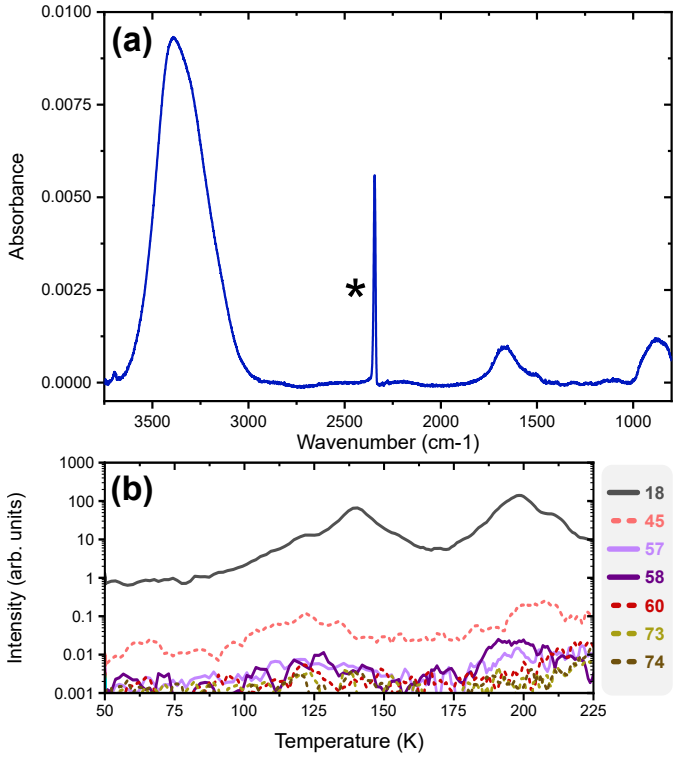


Figure SF8: The IR spectrum and corresponding TPD measurement of oxygen atoms and hydrogen atoms on the gold substrate. (a) shows the IR spectrum with features of water that has formed on the surface and CO_2, marked by *, that had degassed from the atomic dosers and adsorbed onto the surface. (b) shows the corresponding TPD measurement where water can be seen to desorb, with no other traces of acids or aldehydes.

Supplementary Fig SF8(a) shows the IR spectrum of the oxygen and hydrogen atom dose. The strong, broad band, centred at 3386 cm^{-1}, is the OH stretching mode of water [12]. The formation of water is expected, as it is known that the combination of these atoms leads to a series of reactions terminating with H_2O [13]. The other modes expected for water are also present, with the OH bending mode at 1667 cm^{-1} and the libration mode at 877 cm^{-1} [12]. This water formation was also observed for the experiments where propanal was exposed to OH, and for pentanal exposed to OH, shown in Fig 6. Also shown in this figure, marked with *, is a band assigned to the asymmetric stretch of CO_2 [14]. This isn't formed on the surface and is therefore most likely due to the atom dosers degassing while they are heated. This was also observed for each experiment that exposed either propanal or pentanal to oxygen atoms or OH molecules. This shows that the detected CO_2 is from deposition and not due to chemical reactions on the surface and can therefore be discounted in the measurements.

Supplementary Fig SF8(b) shows the TPD traces of the oxygen and hydrogen atom dose. Included are the masses that were investigated for water (18 amu), propanal (57, 58 amu) [15], propanoic acid(45, 73, and 74 amu) [16], pentanal (57, 58 amu) [9], and pentanoic acid (60, 73 amu) [10]. Water can be seen to desorb from the surface at 140 K, with a sample holder peak at 198 K showing that it was formed

in this reaction. The other mass traces show no significant increase or desorption peaks, meaning that those signals measured in other traces come from reactions on the surface and not from the doser.

References

[1] Yarnall, Y. Y., Gerakines, P. A. & Hudson, R. L. Propanal, an interstellar aldehyde - first infrared band strengths and other properties of the amorphous and crystalline forms. *mnras* **494**, 4606–4615 (2020).

[2] Jakobsen, R., Mikawa, Y., Allkins, J. & Carlson, G. The vibrational spectra of propanoic acid. *Journal of Molecular Structure* **10**, 300–303 (1971). URL https://www.sciencedirect.com/science/article/pii/0022286071870898.

[3] Peng, Y., Jiang, Z. & Chen, J. Mechanism and kinetics of methane combustion, part i: Thermal rate constants for hydrogen-abstraction reaction of ch4 + o(3p). *The Journal of Physical Chemistry A* **121**, 2209–2220 (2017). URL https://doi.org/10.1021/acs.jpca.6b12125. PMID: 28248505.

[4] Lamberts, T., Fedoseev, G., Kästner, J., Ioppolo, S. & Linnartz, H. Importance of tunneling in h-abstraction reactions by oh radicals-the case of ch4+ oh studied through isotope-substituted analogs. *Astronomy & Astrophysics* **599**, A132 (2017).

[5] Carder, J. T., Ochs, W. & Herbst, E. Modelling the insertion of o(1d) into methane on the surface of interstellar ice mantles. *Monthly Notices of the Royal Astronomical Society* **508**, 1526–1532 (2021). URL https://doi.org/10.1093/mnras/stab2619.

[6] Hickson, K. M. & Loison, J.-C. Kinetic study of the gas-phase o(1d) + ch3oh and o(1d) + ch3cn reactions: Low-temperature rate constants and atomic hydrogen product yields. *The Journal of Physical Chemistry A* **126**, 3903–3913 (2022). PMID: 35687018.

[7] Bates, D., Esselman, B. J., Schultz, C. P. & Widicus Weaver, S. L. Theoretical investigation of the reaction of o(1d) with formamide. *The Journal of Physical Chemistry A* **128**, 9426–9432 (2024). URL https://doi.org/10.1021/acs.jpca.4c05611. PMID: 39432261.

[8] Hays, B. M. & Widicus Weaver, S. L. Theoretical examination of o(1d) insertion reactions to form methanediol, methoxymethanol, and aminomethanol. *The Journal of Physical Chemistry A* **117**, 7142–7148 (2013). URL https://doi.org/10.1021/jp400753r. PMID: 23646865.

[9] NIST Mass Spectrometry Data Center. Pentanal (2025). URL https://webbook.nist.gov/cgi/cbook.cgi?ID=C110623Mask=200Mass-Spec.

[10] NIST Mass Spectrometry Data Center. Pentanoic acid (2025). URL https://webbook.nist.gov/cgi/cbook.cgi?ID=C109524Mask=200Mass-Spec.

[11] Leitner, T., Kattner, J. & Hoffmann, H. Infrared reflection spectroscopy of thin films on highly oriented pyrolytic graphite. *Applied spectroscopy* **57**, 1502–1509 (2003).

[12] Noble, J. A., Cuppen, H. M., Coussan, S., Redlich, B. & Ioppolo, S. Infrared resonant vibrationally induced restructuring of amorphous solid water. *The Journal of Physical Chemistry C* **124**, 20864–20873 (2020). URL https://doi.org/10.1021/acs.jpcc.0c04463.

[13] Jing, D. *et al.* On Water Formation in the Interstellar Medium: Laboratory Study of the O+D Reaction on Surfaces. *apjl* **741**, L9 (2011).

[14] Suhasaria, T., Leuschner, V., Jäger, C., Gieser, C. & Henning, T. Co2 infrared spectra on silicate dust grain analogs: Implications for jwst observations. *The Astrophysical Journal Letters* **988**, L27 (2025). URL https://doi.org/10.3847/2041-8213/ade993.

[15] NIST Mass Spectrometry Data Center. Propanal (2025). URL https://webbook.nist.gov/cgi/cbook.cgi?ID=C123386Mask=200Mass-Spec.

[16] NIST Mass Spectrometry Data Center. Propanoic acid (2025). URL https://webbook.nist.gov/cgi/cbook.cgi?ID=C79094Mask=200Mass-Spec.